Visualization of Marangoni Convection in Simulated Weld Pools

Marangoni convection resembling that in weld pools is revealed by flow visualization

BY C. LIMMANEEVICHITR AND S. KOU

ABSTRACT. A transparent pool of $NaNO_3$ (10 mm in diameter) was heated with a defocused CO_2 laser beam to simulate Marangoni convection in arc weld pools without a surface-active agent. The flow patterns were revealed clearly by flow visualization with a laser light-cut technique, the surface temperature profiles were measured immediately below the pool surface, and a device for measuring the beam diameter was developed. The observed Marangoni convection was expected to resemble that in welding because the Marangoni number was close to those in welding. Two counterrotating cells were observed in the meridian plane of the pool. The maximum velocity was at the pool surface, the outward surface flow was much faster than the inward return flow and the centers of the cells were near the pool edge. These characteristics suggest Marangoni convection dominates in the pool over gravity-induced convection. Increasing the beam power (from 0.5 to 5.4 W) and reducing the beam diameter (from 5.9 to 1.5 mm) both made Marangoni convection stronger. The latter, however, had a significantly greater effect; the surface flow was so much stronger as to make the return flow penetrate deeper into the pool. The results of physical simulation provided interesting insights for understanding the significant effect of Marangoni convection on the weld pool shape, as will be presented in a follow-up report.

Introduction

Marangoni convection, also called surface-tension-driven convection or thermocapillary convection, in the weld pool is of practical interest in welding. It can have a dramatic effect on the penetration depth of the resultant weld (Ref. 1). Marangoni convection in a weld pool without a surface-active agent is illustrated in Fig. 1. The surface-active agent of a liquid, *e.g.*, S in liquid steel, is a material that can significantly reduce the surface tension of the liquid and even change its temperature dependence. As shown by the velocity profile, fluid flow near the pool surface is outward, with the maximum velocity v_s located at and tangent to the pool surface, where the subscript, s, denotes the tangent direction. The outward-pointing shear stress at the pool surface, τ_{ns} ($= -\mu\partial v_s/\partial n > 0$), is induced by the surface-tension gradients along the pool surface $\partial\gamma/\partial s$ (> 0), where n denotes the normal direction, μ is the viscosity and γ is the surface tension. These surface-tension gradients $\partial\gamma/\partial s (= \partial T/\partial s \times \partial\gamma/\partial T)$ are induced both by the temperature gradients along the pool surface $\partial T/\partial s$ (<0) and the temperature dependence of the surface tension $\partial\gamma/\partial T$ (<0). The fluid is pulled along the pool surface from the center (where temperature is high and the surface tension is low) to the edge (where temperature is low and the surface tension is high). Herein, the outward flow along the pool surface will be called the surface flow and the inward flow in the interior of the pool will be called the return flow.

KEY WORDS

Arc Welding
Buoyancy Convection
Flow Visualization
Laser Beam
Marangoni Convection
Surface-Active Agent
Weld Pool

The presence of a very small amount of a surface-active agent can make the weld pool much deeper (Ref. 1). Thermodynamics can show that in the presence of such an agent, the surface tension can, in fact, increase with increasing temperature, *i.e.*, $\partial\gamma/\partial T > 0$ (Ref. 2). With the direction of flow reversed to favor convective heat transfer from the heat source to the pool bottom, a much deeper pool can be produced (Ref. 1). General information about Marangoni convection in the weld pool is available elsewhere (*e.g.*, Refs. 3, 4).

Marangoni convection cannot be studied in arc welding because of the interference by the electromagnetic force in the weld pool and by the aerodynamic drag force of the arc. To avoid this problem, the arc can be substituted with a laser beam defocused to the size of the arc, as illustrated in Fig. 1. As in arc welding, melting is through heating from the top surface (the so-called conduction mode) and no vapor hole is produced in the weld pool by the laser beam (the so-called keyholing mode). The Marangoni convection induced by such a defocused laser beam should be similar to that induced by a welding arc.

Flow visualization in a weld pool is limited to the pool surface because the molten metal is opaque. In fact, even at the pool surface such observation can still be difficult because of the brightness of the arc. Ishizaki, *et al.* (Ref. 5), observed Marangoni convection in a thin slice of molten paraffin heated by a soldering iron in contact with its top surface. The flow pattern was two-dimensional rather than axisymmetrical and was not clearly revealed.

In the present investigation, Marangoni convection in weld pools without a surface-active agent is simulated using a transparent pool of $NaNO_3$. Unlike paraffin, which is often a mixture

C. LIMMANEEVICHITR and S. KOU are graduate student and Professor, respectively, in the Department of Materials Science and Engineering, University of Wisconsin, Madison, Wis.

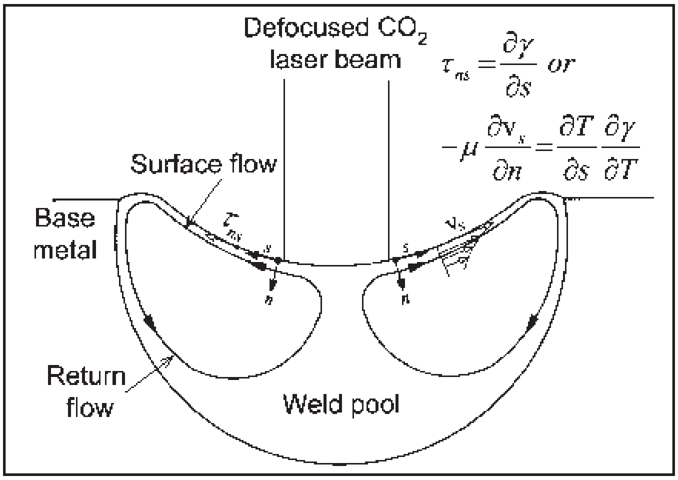

Fig. 1 — Marangoni convection in a weld pool induced by a laser beam defocused to the size of an arc.

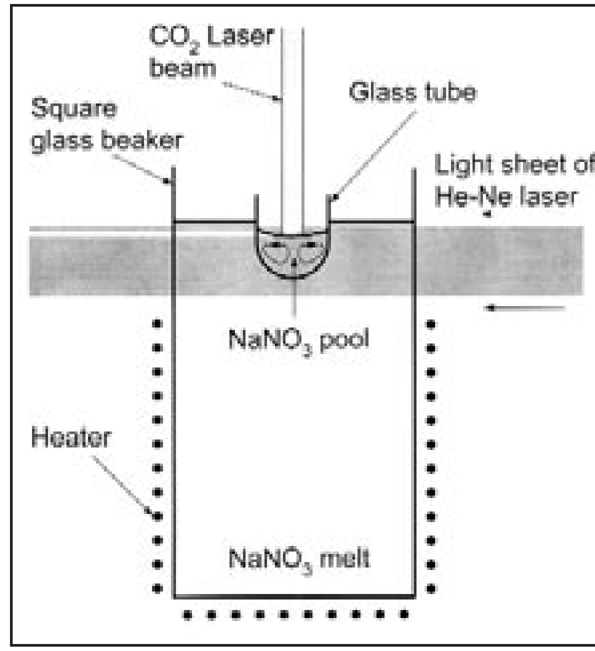

Fig. 2 — A transparent system for physical simulation of Marangoni convection in a weld pool, with the outer $NaNO_3$ melt keeping the pool molten and clear, and correcting optical distortions caused by the lens effect of the pool.

of several organic compounds, the physical properties of $NaNO_3$ are well documented. Furthermore, a CO_2 laser beam rather than a soldering iron is used as the heat source to avoid interfering with flow in the pool and distorting the free surface and the flow pattern. To clearly reveal the flow pattern in the pool, a laser-light cut technique is used and optical distortions due to the lens effect of the pool are carefully eliminated.

The objectives of the present study are to observe Marangoni convection in a simulated weld pool and to understand the effect of the power and diameter of the heat source on such flow. The results will be used to explain the effect of the heat source and the Prandtl number Pr on the shape of stationary weld pools. Due to space limitations, this will be dealt with separately in a subsequent paper. Oscillatory flow is beyond the scope of the present study.

Experimental Procedure

Materials

Sodium nitrate, $NaNO_3$, was selected as the material for flow visualization because of the following reasons. First, $NaNO_3$ has a transparent melt, a surface tension that significantly varies with temperature, a low melting point and well-documented physical properties, as shown in Table 1 (Refs. 6–10). Second, as will be described in the Results and Discussion section of this paper, the Marangoni number Ma for the simulated $NaNO_3$ weld pool to be studied here is close to those for steel and aluminum weld pools. According to the similarity law of hydrodynamics, similarity in Marangoni convection between two fluid systems can be expected if the Marangoni numbers are close to each other (Ref. 11). Third, $NaNO_3$ has a transmission range of 0.35–3 μm and is, therefore, opaque to a CO_2 laser (10.6 μm) just like a weld pool is opaque to the heat source. The purity of the $NaNO_3$ used was above 99%.

Apparatus

The apparatus for flow visualization, shown in Fig. 2, consisted of the following components. First, an essentially hemispherical pool of $NaNO_3$ was held in a glass tube (10-mm ID). Second, a much larger $NaNO_3$ melt was held in a square glass beaker (40 mm x 40 mm inside) to keep the pool from freezing and becoming opaque. Third, a CO_2 laser beam was shone at the center of the pool surface to induce Marangoni convection. Fourth, a He-Ne laser light sheet was passed through the meridian plane of the pool as an illuminator to reveal the flow pattern.

The glass containers were mounted on an x-y table to help align the center of the pool surface with the CO_2 laser beam. The glass tube, 15 mm long and with a 0.5-mm wall, was lowered 8 mm into the $NaNO_3$ melt. A thermocouple placed in the glass beaker near the bottom of its wall was hooked up to a temperature controller set at 330°C. In the absence of a CO_2 laser beam, this gave a temperature of 323.4°C at the bottom of the outer surface of the glass tube.

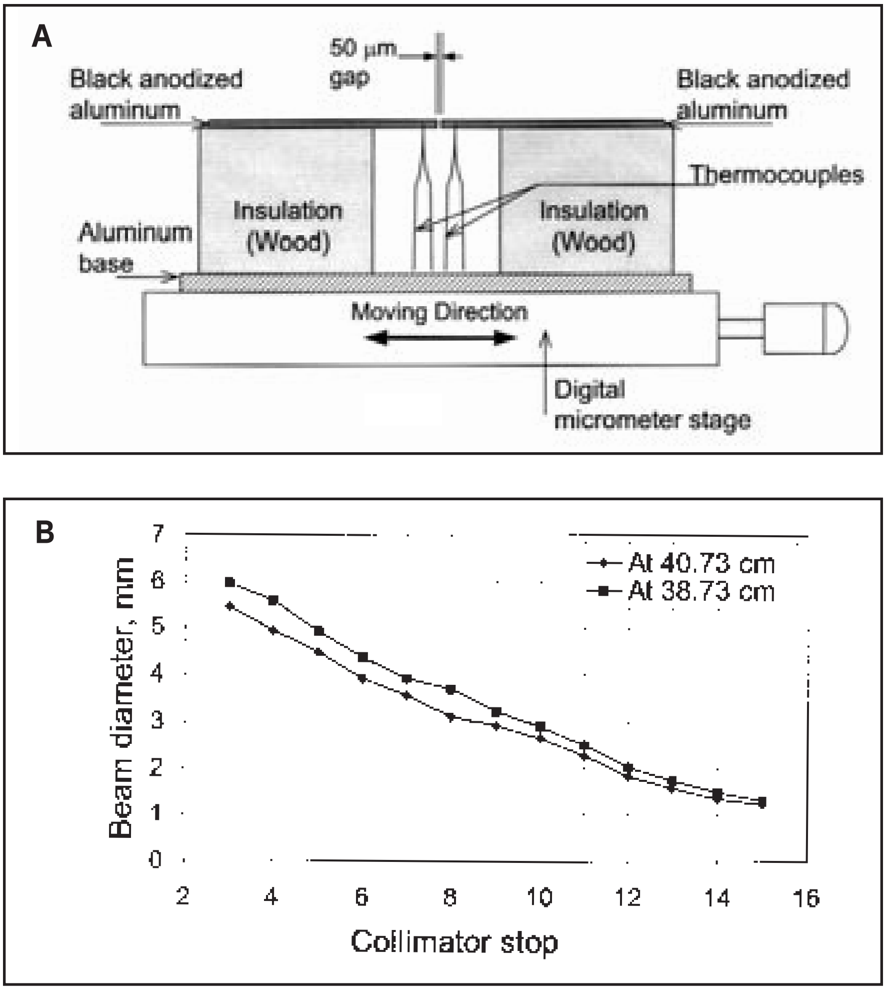

Fig. 3 — Measurement of the diameter of a CO_2 laser beam: A — The device developed in the present study; B — results obtained at two different distances below the beam bender.

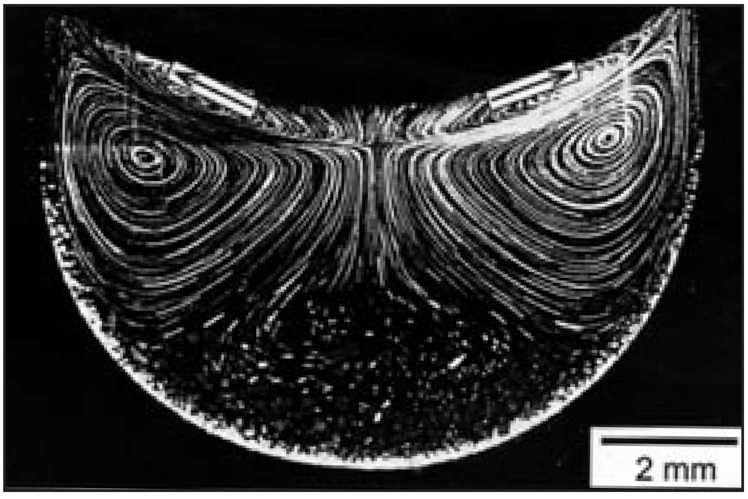

Fig. 4 — Flow pattern induced by a CO_2 laser beam of 2.5 W and 3.2 mm diameter.

While flow visualization in water is easy to do, flow visualization in a melt at an elevated temperature can be tricky. The apparatus is unique in that it was transparent and free from optical distortions, as described in the following:

1) The heater keeping the $NaNO_3$ pool from freezing was transparent. This heater was the $NaNO_3$ melt surrounding the pool and was itself heated by a Nichrome-wire heater positioned below the laser light sheet to avoid blocking the view. Both the tube and the beaker were transparent Pyrex glass.

2) The heater corrected the severe optical distortions in the observed flow patterns by eliminating the lens effect of $NaNO_3$ (refractive index n = 1.46). The $NaNO_3$ pool was, in fact, an optical lens. To correct this lens effect, the glass beaker was made square rather than round. Furthermore, the difference between the refractive index of the $NaNO_3$ melt and that of Pyrex glass (n = 1.47) is too small to cause any additional optical distortions in the observed flow patterns. The $NaNO_3$ melt was much larger in volume than the pool in order to make the temperature around the pool stable and uniform.

Experiments were also carried out using a different heat source — a Nichrome wire of 0.76 mm diameter heated by passing an electric current through it. The CO_2 laser alone was replaced by the wire heater; the rest of the system, including the transparent heater surrounding the pool, remained unchanged. The wire was bent into the shape of a sharp V, and the bottom end of the V was lowered to touch the center of the pool surface. A 0.25-mm-diameter K-type thermocouple was spot welded to the bottom of the V from the side to measure its temperature.

Beam-Diameter Measurement

The CO_2 laser had a wavelength of 10.59 μm, power stability of ± 5%, beam quality of $M^2 < 1.2$ and beam mode of TEM_{00} and 90% purity (better than 90% Gaussian), where M is the magnification factor. The raw beam diameter was 4.4 mm, and the beam divergence was 3.2 mR. A beam bender deflected the horizontal laser beam downward. A two-lens beam collimator with 15 stops available for varying the beam diameter was mounted under the beam bender. The beam power was measured with a power meter having a 0.1-W resolution.

To measure the beam diameter, the device shown in Fig. 3A was prepared. To increase absorption of the beam power, a black anodized aluminum sheet, 58 mm long x 20 mm wide x 2 mm thick, was used to receive the laser beam. Two K-type thermocouples were mounted 3 mm from each other at the center of the black anodized aluminum sheet from its bottom. This aluminum sheet was bonded to two wood blocks, which served as a thermal insulator and which themselves were bonded to an aluminum base. The anodized aluminum sheet was then cut in the middle with a precision wire saw with a 50-μm-diameter tungsten wire. A smaller wire, *e.g.*, 10 μm diameter, can be used if smaller beams are to be measured. The whole assembly was then mounted on a digital micrometer stage that could be reset to zero at any position.

The device was positioned so the top surface of the anodized aluminum was at the height where the beam diameter was to be measured, *i.e.*, at the level where the center of the pool surface was expected in subsequent flow visualization experiments. This level was 38.7 cm below the beam bender. With a 3-W CO_2 laser beam shining on the left half of the anodized aluminum, the micrometer stage was moved to the left until the right thermocouple sensed a quick, clear temperature rise. The micrometer was reset to zero at this position and the system was cooled to room temperature with an air gun. The micrometer stage was then moved farther to the left until the laser beam could shine only on the right half of the anodized aluminum. With the laser beam shining on the right half of the anodized aluminum, the micrometer stage was moved to the right until the left thermocouple sensed a similar temperature rise. This position reading of the micrometer stage was taken as the beam diameter. The micrometer stage was then turned 90 deg and the beam diameter was measured in the new direction following the same procedure. The average of the two measurements was taken as the beam diameter. This procedure was repeated for all stops of the beam collimator. The beam diameter was also measured at 40.7 cm below the beam bender.

Flow Visualization

A laser light-cut technique for flow visualization was used. The laser light sheet was produced with the help of a 20-mW He-Ne laser and optical lenses. Aluminum particles 20 μm in diameter were used as a tracer. The density of aluminum (2.7 g cm^{-3}) is greater than that of the $NaNO_3$ melt (1.9 g cm^{-3}). From Stokes's law (Ref. 4), however, the settling velocity is much slower than Marangoni convection in view of the small particle diameter. In fact, aluminum particles are often used for flow visualization in water (Ref. 12), which is even lighter than $NaNO_3$. A certain amount of aluminum particles gradually settled to the pool bottom over extended periods of time. Photographs of the flow patterns were taken at the exposure time of 0.625 s, with the reflex mirror of the camera locked to reduce vibration.

Surface Temperature Measurement

The surface temperature profiles near the pool surface were measured with a K-type thermocouple. It was prepared from 0.05-mm (0.002-in.) diameter wires with an exposed bead 0.125 mm (0.005 in.) in diameter. To minimize interference with flow, the thermocouple was bent into a J shape to conform to the pool wall and axis. With the help of a digital micrometer x-y stage and a magnifying lens, the tip of the thermocouple was positioned at 0.125 mm below the pool surface.

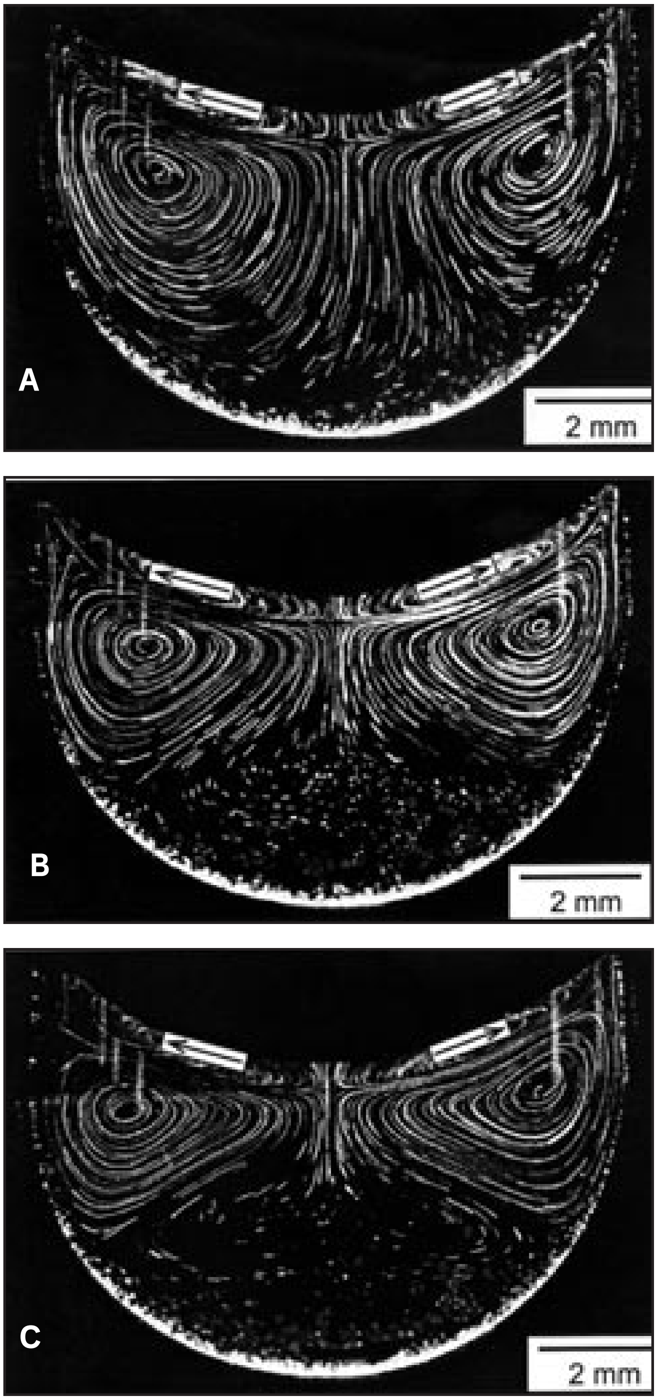

Fig. 5 — Flow patterns induced by a CO_2 laser beam of 5.9 mm diameter at the following power levels: A — 0.5 W; B — 2.5 W; C — 5.4 W. Fluid flow becomes faster but shallower as the power is increased.

Results and Discussion

Diameter of Heat Source

In numerical simulation of heat and fluid flow in the weld pool, the power-density distribution of the heat source is often assumed Gaussian and the effective diameter of the heat source is often defined as the diameter that covers 95% of the total power of the heat source (Ref. 13). The simple device developed in the present study measures an effective beam diameter within which heating can be detected with a thermocouple. It does not specify which kind of definition the effective diameter is based on. The precise definition of the effective beam diameter, however, is not critical because the focus here is to demonstrate the effect of the beam diameter on Marangoni convection, and the conclusions drawn will not

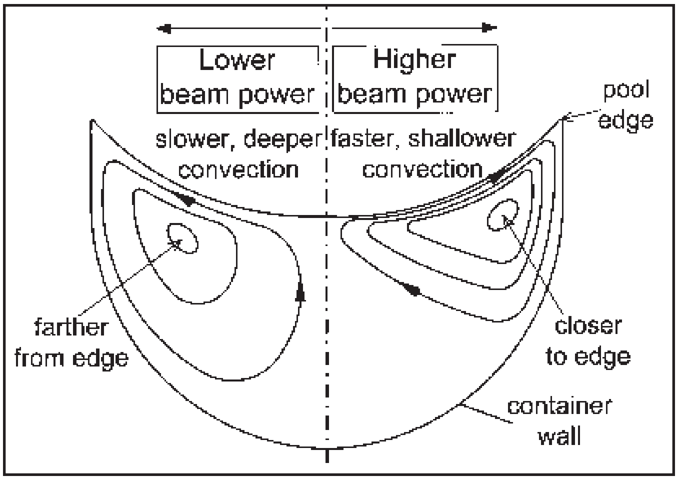

Fig. 6 — Effect of the power of the laser beam on the flow pattern.

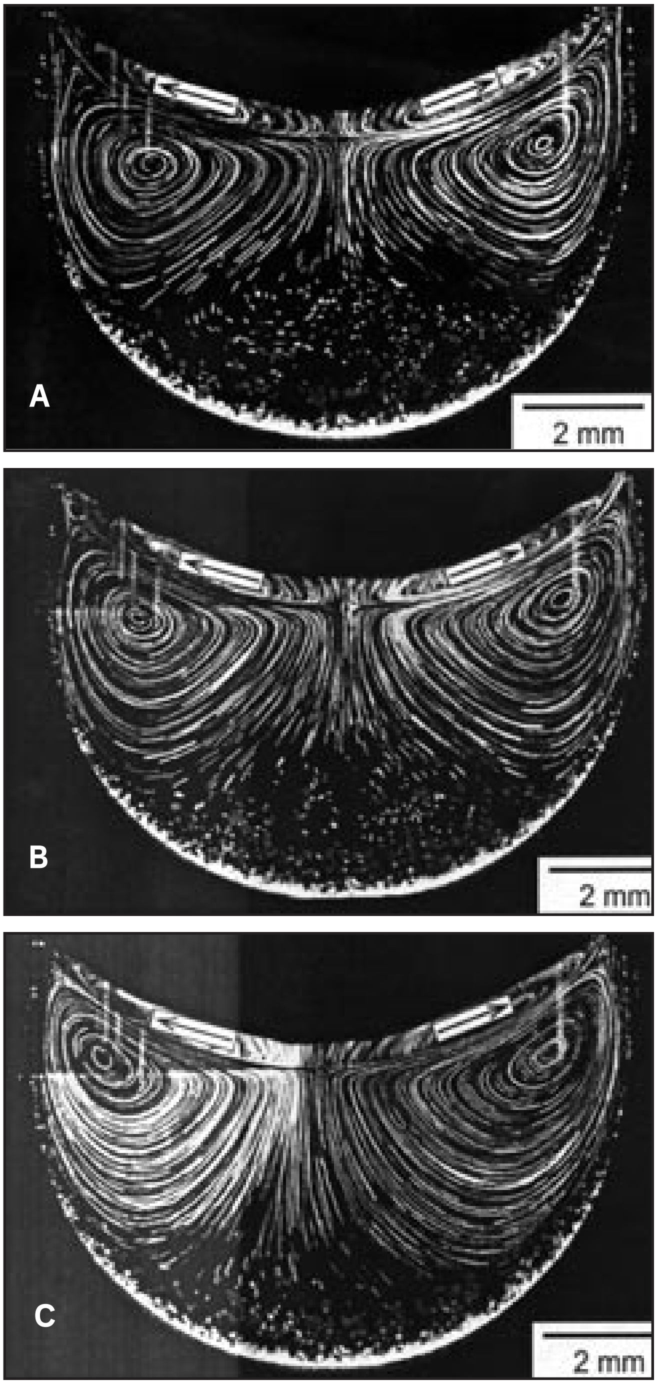

Fig. 7 — Flow patterns induced by a 2.5-W CO_2 laser beam at the following diameters: A — 5.9 mm; B — 3.2 mm; C — 1.5 mm. Fluid flow becomes faster and deeper as the beam diameter is reduced.

be affected by how precisely the beam diameter is defined. Both the actual power density distribution of the heat source and its effective diameter, however, can be determined if desired. This can be done by determining the amount of power absorbed by each of the two anodized aluminum sheets while they are being traversed under the heat source at a constant slow speed (Ref. 14). The power density distribution can be obtained with the help of Abel transformation. This, however, is no trivial task. Commercial instruments might be available but rather expensive.

Figure 3B shows the results of beam diameter measurements at 38.7 and 40.7 cm below the beam bender. As shown, with the center of the pool surface positioned at 38.7 cm below the beam bender, the beam diameter can be varied from about 1.3 to 5.9 mm, which is close to the diameter of a gas tungsten arc.

Three beam diameters were used in the present study: 1.5, 3.2 and 5.9 mm. The 5.9-mm beam diameter seems a reasonable upper boundary considering the already small clearance of about 2 mm between the beam and the inner wall of the 10-mm-ID glass tube holding the pool.

Flow Pattern

Figure 4 shows the flow pattern induced by a CO_2 laser beam of 2.5 W power and 3.2 mm diameter. It is worth noting the pool surface in conduction-mode laser beam welding can be concave due to Marangoni convection and surface tension (Ref. 15), and, in fact, this has been shown to be the case experimentally (Ref. 16) and by computer simulation (Ref. 17). The concave pool surface shown in Fig. 4, however, is just a coincidence; the melt wets the container wall and forms a meniscus to make the pool surface concave.

The arrows above the pool surface indicate the directions of flow along the pool surface. The flow lines above the pool surface are not real but are only the image of the flow lines inside the pool. The concave free surface acts as a mirror and shows the flow lines that are inside the pool.

Fluid flow is steady, axisymmetric and essentially unicellular, though it is not clear if there are much weaker secondary cells near the pool bottom. In the meridian plane of the pool, however, the flow pattern appears as a clockwise cell on the right and a counterclockwise cell on the left. In other words, the melt at the center of the pool surface flows outward along the pool surface, turns downward at the pool edge to fall along the pool wall and then returns to the center of the pool surface.

The flow lines are most closely spaced near the pool surface and become more widely separated below the pool surface and in the bulk pool. The top of the right half of the pool in Fig. 4 is particularly clear in showing that the flow lines converge near the pool surface. There is little flow in the area near the bottom of the pool. The centers of the cells are near (0.9 mm below) the pool surface and close to (1.4 mm from) the wall. Therefore, it appears the maximum velocity is at the pool surface (as illustrated in Fig. 1), the sur-

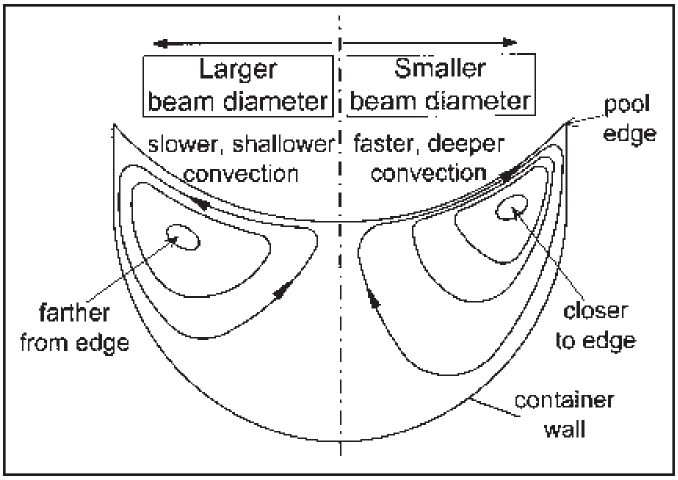

Fig. 8 — Effect of the diameter of the laser beam on the flow pattern.

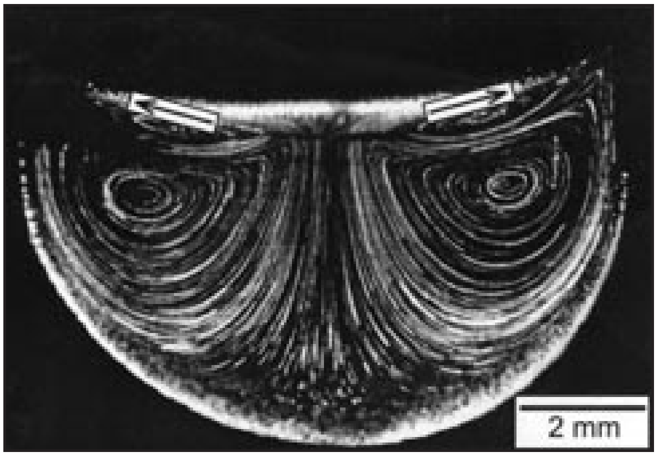

Fig. 9 — Flow pattern induced by a wire heater touching the center of the pool surface, the heater being 48.6°C higher in temperature than the pool edge.

face flow is much faster than the return flow and the centers of the cells are close to the pool edge. The videotape recorded during flow visualization (Ref. 18) confirms these characteristics of Marangoni convection. Therefore, it is clear Marangoni convection dominates over bouyancy convection.

Effect of Heat Source Power

Three levels of the beam power are used in the present study: 0.5, 2.5 and 5.4 W. Further increase in power tends to cause oscillatory flow, especially at small beam diameters.

Figure 5 shows the effect of the beam power on fluid flow at the beam diameter of 5.9 mm. At 0.5 W fluid flow is slow, unsteady and lacking axisymmetry, as shown in Fig. 5A. Since the surface flow is slow, the return flow appears to have plenty of time to fall to near the pool bottom before rising to the pool surface. Buoyancy convection is expected to play a significant role in view of the weak Marangoni convection.

At 2.5 W, fluid flow is significantly faster, steady and essentially axisymmetrical, and the centers of the cells move closer to the edge of the pool surface, as shown in Fig. 5B. However, the cells are now shallow penetrating and, in fact, look more triangular than round. Since the surface flow is faster now, the return flow also has to be faster to satisfy the continuity requirement. Instead of falling near the pool bottom and then rising to the pool surface, which takes time, the return flow appears to take a shortcut back to the pool surface.

At 5.4 W, fluid flow is even faster. The cells are even more shallow penetrating and triangular, and the centers of the cells move even closer to the edge of the pool surface, as shown in Fig. 5C. Similar experiments conducted at the 3.2- and 1.5-mm beam diameters show a similar effect of the beam power.

The effect of increasing the beam power is summarized in Fig. 6. As the beam power is raised from 0.5 to 5.4 W at the constant beam diameter of 5.9 mm, flow becomes significantly faster and the centers of the cells move closer to the pool edge. The faster surface flow requires a faster return flow to satisfy continuity, and the return flow takes a shortcut back to the pool surface instead of reaching the pool bottom. This results in shallow-penetrating, triangular cells.

In a real weld pool, the pool diameter is not fixed but allowed to increase as the power is increased. The effect of this will be discussed later in this paper.

The authors are not aware of any numerical simulations that have predicted the effect of the beam power observed here. However, Kamotani, *et al.* (Ref. 19), have conducted numerical simulation of Marangoni convection in a liquid that is held in a cylindrical container with a flat bottom and that is heated by a laser at the center of the free surface. The calculated streamlines show cells similar to those observed in the present study. Furthermore, as Marangoni convection becomes stronger, the cells become shallower and more triangular, and the centers of the cells move closer to the pool edge.

Effect of Heat Source Diameter

Figure 7 shows the effect of the beam diameter on fluid flow at the power level of 2.5 W. Figure 7A, which shows the flow pattern induced by a 5.9-mm beam, is identical to Fig. 5B. As already mentioned, the cells are shallow and triangular.

With the beam diameter reduced to 3.2 mm, Marangoni convection becomes significantly faster and, as shown in Fig. 7B, the centers of the cells move closer to the pool edge. The surface flow now accelerates more sharply toward the pool edge. This gives the return flow more momentum to penetrate deeper into the pool, even though this means the return flow has to travel a longer distance and at a higher velocity back to the pool surface.

With the beam diameter further reduced to 1.5 mm, the surface flow accelerates even more sharply. As shown in Fig. 7C, the return flow now penetrates even deeper into the pool. Having to return to the pool surface with a much higher velocity, the return flow turns abruptly near the pool surface. Similar experiments conducted at 0.5 and 5.4 W show a similar effect of the beam diameter.

The effect of reducing the beam diameter is summarized in Fig. 8. As the beam diameter is reduced from 5.9 to 1.5 mm at the constant power of 2.5 W, flow becomes much faster and the centers of the cells move closer to the pool edge. The return flow gains extra momentum to penetrate deeper into the pool.

Again, in a real weld pool, the pool diameter is not fixed but allowed to increase as the power is increased. The effect of this will also be discussed later in this paper.

The authors are not aware of any numerical simulations that have predicted the effect of the beam diameter observed here, though it is likely such simulations may have been done.

Heater Touching Pool Surface

The advantage of the wire heater is that the temperature difference across the pool surface, which is the driving force

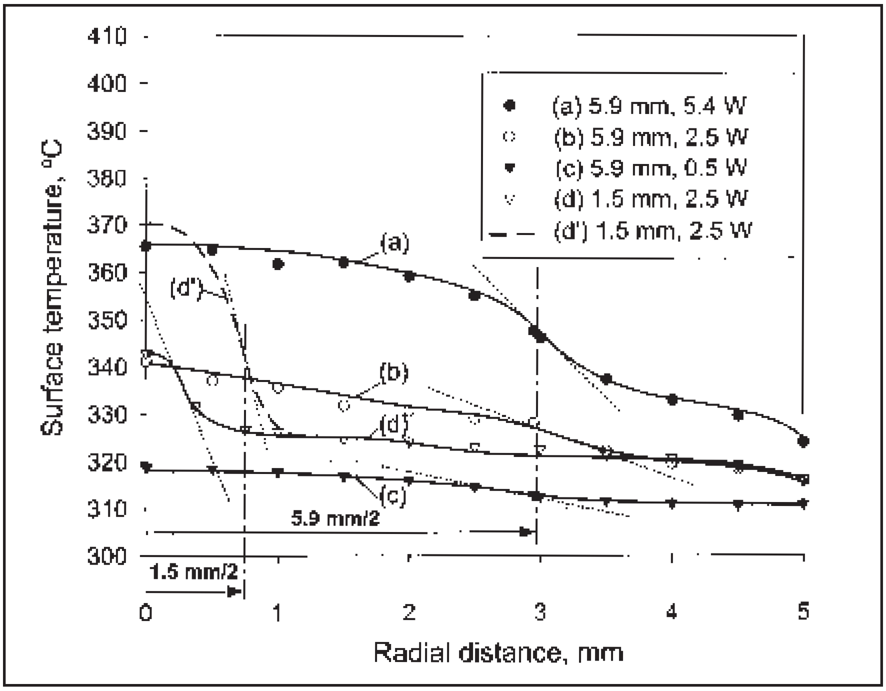

Fig. 10 — Temperature profiles along but slightly below the pool surface at various diameters and power levels of the laser beam. The broken curve shows the projected surface temperature profile for 1.5-mm diameter and 2.5-W power. Dotted lines are tangents showing the maximum radial temperature gradients.

for Marangoni convection, can be easily found. Of course, the disadvantage is that, unlike a laser beam, it touches the pool surface, though much less than a soldering iron does.

Figure 9 shows the flow pattern induced by the V-shaped wire heater touching the center of the pool surface. The temperature at the center of the pool surface, as indicated by the thermocouple spot welded to the tip of the heater, was 373.7°C, and the temperature at the pool edge was 325.1°C. As such, the surface temperature was 48.6°C higher at the center than at the pool edge. The flow pattern is closest to that induced by a 2.5-W beam of 1.5 mm diameter — Fig. 7C. The differences, however, are that a hump is formed at the center of the pool surface by the meniscus at the wire heater and the centers of the cells are farther away from the pool edge. More details on the flow patterns induced by the wire heater are available elsewhere (Ref. 20).

Surface Temperature Profiles

The temperature profile along the pool surface is most helpful for understanding Marangoni convection in the pool but difficult to measure with a thermocouple. An alternative is to use an infrared imager, *e.g.*, that used by Kamotani, *et al.* (Ref. 21), to study Marangoni convection in a silicone oil held in a cylindrical container with a flat bottom and heated by a vertical wire along the axis. In the case of silicone oil, the infrared imager detected radiation emitted by a 0.2-mm-thick surface layer. No data are available to verify this is also true in the case of $NaNO_3$. Radiation from the interior of the pool can cause significant errors in measuring the pool surface temperature. Another difficulty is the laser beam is in the way, making overhead imaging over a relatively small $NaNO_3$ pool difficult.

The solid curves in Fig. 10 show the temperature profiles measured along the pool surface — with the tip of the thermocouple positioned at 0.125 mm below the pool surface. All curves are drawn with an essentially zero slope at the center of the pool surface in view of the thermal boundary condition $\partial T/\partial r = 0$ at the axis of symmetry r = 0. The maximum radial temperature gradient $(-\partial T/\partial r)_{max}$ at the pool surface is indicated with a tangent (dotted line) to each curve of the temperature profile.

Curves a through c are the temperature profiles induced by a 5.9-mm-diameter beam. As shown, as the beam power is increased from 0.5 to 5.4 W, the temperature near the center of the pool surface rises more significantly than that near the edge. As such, the temperature difference ΔT between the center and the edge of the pool increases with increasing beam power, and this explains why convection becomes faster when the beam power is increased — Fig. 5. The maximum radial temperature gradient $(-\partial T/\partial r)_{max}$, which occurs around the edge of the laser beam, increases from about 4 to 11 and 21°C/mm as the beam power increases from 0.5 to 2.5 and 5.4 W, respectively.

Curves b and d show the temperature profiles induced by a beam power of 2.5 W. As the beam diameter is reduced from 5.9 to 1.5 mm, three things change significantly. First, $(-\partial T/\partial r)_{max}$ increases from about 11 to 50°C/mm. Second, the radial position of $(-\partial T/\partial r)_{max}$ is no longer about 3 mm from the center of the pool surface, but much closer at about 0.3 mm. Third, the power density q_z rises sharply by a factor of $(5.9/1.5)^2$ or 15.5.

From Fourier's law of conduction, at the pool surface

$$q_z = -k \frac{\partial T}{\partial z} \qquad (1)$$

where q_z is the heat flux due to the laser beam, k the thermal conductivity of the melt and z the distance along the axis of the pool. As an approximation,

$$\frac{Q}{\pi R_h^2} \approx k \frac{(\Delta T)_\delta}{\delta_T} \qquad (2)$$

where Q is the beam power, R_h the beam radius, δ_T the thickness of the thermal boundary layer at the free surface caused by laser heating and $(\Delta T)_\delta$ the temperature drop across δ_T. In view of the very low k of $NaNO_3$ (Table 1), the temperature gradient $\partial T/\partial z$ at the pool surface under the laser beam is expected to be high. As such, the actual surface temperature profiles can be expected to be higher than the measured ones, especially the one for a 1.5-mm beam diameter.

For the case of 2.5-W power and 1.5-mm beam diameter, the temperature measured at 0.125 mm below the center of the pool surface is 343°C, according to Curve d of Fig. 10. The true surface temperature should be between 343°C and the decomposition temperature of 380°C because decomposition was not observed. As such, the true temperature at the center of the pool surface is not expected to be more than about 370°C. This gives a $(\Delta T)_\delta$ of 27°C. From k = 5.65 x 10^{-3} W/cm^{-1}°C^{-1} and Equation 2, δ_T = 0.011 mm (or 11 μm), which is about one-tenth of the distance between the thermocouple and the free surface (0.125 mm). This very small δ_T is a consequence of the very low k plus the impingement of the free surface by the cooler return flow from below. It is interesting to note 370°C happens to be close to the temperature 373.7°C of the heater touching the center of the pool surface — Fig. 9.

The projected surface temperature profile is shown in Fig. 10 by Curve d'. The high ΔT across the pool surface and the high $(-\partial T/\partial r)_{max}$ explain why Marangoni convection becomes much faster and deeper as the beam diameter is reduced from 5.9 to 1.5 mm — Fig. 7. This surface temperature profile is similar to those calculated by Kamotani, *et al.* (Ref. 19), for laser-beam-induced Marangoni convection in silicone oil held in a cylindrical container. There, the surface temperature decreases with increasing radius, but not at a constant rate across the free surface. The surface temperature drops sharply near the edge of the laser beam but beyond this point it does not decrease much at all, especially when Marangoni convection is significant (Ma close to and greater than 1 x 10^4). In the presence of significant Marangoni convection, the calculated temperature field in the pool shows a very thin thermal boundary layer at the pool surface under the laser beam. $\partial T/\partial z$ is very high within the boundary layer but much lower beyond it.

For the case of 5.9-mm beam diameter, q_z is much lower and the measured surface temperature profiles, Curves a through c, are more accurate. If the same δ_T of 0.011 mm is used, $(\Delta T)_\delta$ is less than 4, 2 and 0.5°C at 5.4, 2.5 and 0.5 W, respectively.

Marangoni Number and Marangoni Convection

The Marangoni number, which has been used widely as a measure for the extent of Marangoni convection, is a dimensionless number defined as

$$Ma = \frac{-\frac{\partial \gamma}{\partial T}(\Delta T)L}{\mu \alpha} \qquad (3)$$

where $\partial\gamma/\partial T$ is the temperature coefficient of surface tension, ΔT the temperature difference between the center and edge of the pool surface, L the characteristic length, μ the dynamic viscosity and α the thermal diffusivity.

From Curve d' in Fig. 10, ΔT = 55°C for a 2.5-W laser beam of 1.5-mm diameter. The characteristic length L can be taken as the pool radius 5 mm. From Equation 3 and the physical properties given in Table 1, the Marangoni number Ma = 2.93 x 10^4.

From computer simulation of heat and fluid flow in stationary weld pools of steel (Refs. 22–24), L is about 4 mm (from 3 to 5 mm) and ΔT is about 750°C (from 500 to 1000°C). Also, μ is about 5 x 10^{-2} g $cm^{-1}s^{-1}$ and α is about 5 x 10^{-2} cm^2 s^{-1}. For a steel with a negligible amount of sulfur, $\partial\gamma/\partial T$ can be taken as –0.3 dyne cm^{-1}°C^{-1} (Ref. 24). From Equation 3, Ma = 3.60 x 10^4, which is of the same order of magnitude as Ma = 2.93 x 10^4 for the simulated weld pool.

Similarly, Tsai, *et al.* (Ref. 17), calculated heat and fluid flow in a stationary aluminum weld pool produced by a defocused laser beam. There, L = 3 mm, ΔT = 850°C and $\partial\gamma/\partial T$ = –0.35 dyne cm^{-1}°C^{-1}. In addition, μ = 1 x 10^{-2} g cm^{-1} s^{-1} and α = 3.75 x 10^{-1} cm^2 s^{-1}. From Equation 3, Ma = 2.38 x 10^4. This, again, is of the same order of magnitude as Ma = 2.93 x 10^4 for the simulated weld pool of $NaNO_3$.

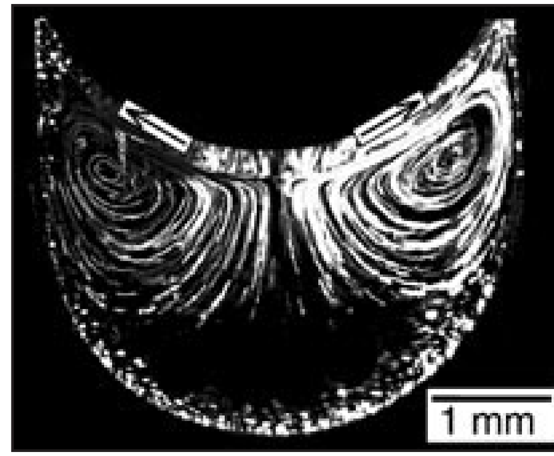

Fig. 11 — Flow pattern in a 4-mm-diameter pool induced by a 2-W laser beam of 1.5 mm diameter.

Heat and fluid flow in a stationary aluminum weld pool produced by a gas tungsten arc has been calculated by Kou, *et al.* (Ref. 13). There, L = 3 mm and ΔT = 1050°C. Based on the same physical properties mentioned before and Equation 3, Ma = 2.94 x 10^4, which again is of the same order of magnitude as Ma = 2.93 x 10^4 for the simulated weld pool of $NaNO_3$.

As such, the Marangoni convection observed in the simulated weld pool can be expected to be similar to that in stationary weld pools produced by a defocused laser beam or an arc. According to the similarity law of hydrodynamics (Ref. 11), similarity in Marangoni convection between two different fluid systems of similar shapes can be expected if the Marangoni numbers are close to each other. The flow pattern in Fig. 4 is consistent with the calculated flow patterns (Refs. 13, 17, 22–24) in the following ways. First, the centers of the cells are near the pool edge; second, the maximum velocity is at the pool surface; and third, the surface flow is much faster than the return flow.

In the present physical simulation, the laser beam is used primarily to induce thermocapillary convection. In actual welding, however, the heat source has to melt a small portion of the workpiece to produce a weld pool. As such, the heat input required is much greater in welding than in the physical simulation. The high welding heat input causes a ΔT that is much higher than that in the physical simulation, as already shown. However, this difference is very much absorbed by the much higher α of a metal workpiece such as steel or aluminum, as suggested by the definition of Ma according to Equation 3. This is why Ma for the simulated weld pool can still be close to Ma for a weld pool of steel or aluminum. When welding solid $NaNO_3$, a higher heat input is required; for example, 10 W produces a pool of about 8-mm diameter (as opposed to 2.5 W for inducing Marangoni convection in the simulated pool). The corresponding ΔT will be higher (say, by one-third) and L lower (by one-fifth), and so Ma for such a $NaNO_3$ weld pool can still have more or less the same order of magnitude as Ma for the simulated pool.

Effect of Tube Wall

As mentioned previously, in a real weld the pool diameter is not fixed but allowed to change depending on the welding condition. Curves a through c in Fig. 10 indicate the temperature at the pool edge increases by about 12°C when the power of the 5.9-mm-diameter beam increases from 0.5 to 5.4 W, suggesting the pool diameter would increase if it were allowed to. From Equation 3, increasing the pool radius L increases Ma and hence Marangoni convection. Therefore, the effect of increasing the beam power on Marangoni convection is likely to be reduced by the presence of the glass tube.

Curves b and d in Fig. 10, on the other hand, show that decreasing the beam diameter of a 2.5-W laser beam from 5.9 to 1.5 mm hardly changes the temperature at the pool edge at all. As such, reducing the beam diameter is not expected to change the pool radius L significantly, and its effect on Marangoni convection is not affected significantly by the presence of the tube wall. Recent experiments have shown that reducing the beam diameter affects the shape of a $NaNO_3$ weld pool significantly but not the pool diameter (Ref. 26).

Bond Number and Buoyancy Convection

Because of heating by the laser beam, the pool surface is warmer at the center than at the edge. As such, buoyancy convection causes the melt to rise along the pool axis and fall along the wall just like Marangoni convection. It is, therefore, desirable to check if the convection observed in the simulated weld pool is dominated by Marangoni or buoyancy convection.

The dynamic Bond number is a dimensionless number defined as follows:

$$Bo = \frac{\beta \rho g L^2}{-\frac{\partial \gamma}{\partial T}} \quad (4)$$

where β is the thermal expansion coefficient of the melt, ρ the density of the melt, g the gravitational acceleration 980 cm s^{-2}, L the characteristic length taken as the radius of the pool and ∂γ/∂T the temperature coefficient of the surface tension. The dynamic Bond number Bo is often used as a qualitative indication of the strength of buoyancy convection relative to that of Marangoni convection.

From computer simulation of heat and fluid flow in stationary weld pools of steel (Refs. 22–24), L is about 4 mm, β is 1 x 10^{-4}°C^{-1}, ρ is 7.2 g cm^{-3}. As already mentioned, for a steel with a negligible amount of sulfur, ∂γ/∂T can be taken as –0.3 dyne cm^{-1}°C^{-1} (Ref. 24). From Equation 4, Bo = 0.38. From computer simulation of heat and fluid flow in stationary weld pools of aluminum (Refs. 13, 17), L is about 3 mm, β is 1 x 10^{-4}°C^{-1}, ρ is 2.7 g cm^{-3} and ∂γ/∂T is –0.35 dyne cm^{-1}°C^{-1}. From Equation 4, Bo = 0.068. Therefore, in welding, Marangoni convection dominates over buoyancy convection.

For a 10-mm-diameter $NaNO_3$ pool, the thermal expansion coefficient of the melt β is 6.6 x 10^{-4}°C^{-1}, the density of the melt ρ is 1.90 g cm^{-3}, the gravitational acceleration g is 980 cm s^{-2}, the characteristic length L is taken as the radius of the pool 0.5 cm and the temperature coefficient of surface tension ∂γ/∂T is –0.056 dyne cm^{-1}°C^{-1}. From these values and Equation 4, Bo = 5.5 for a 10-mm-diameter pool. This is believed to be an overestimate of the importance of buoyancy convection because the characteristics of the flow in the pool (Fig. 4) suggest predominance of Marangoni convection, as described previously.

To reduce the Bond number, experiments with a smaller pool of 4 mm diameter were attempted. From Equation 4, the dynamic Bond number Bo for a 4-mm-diameter pool is 0.88. This is more than six times smaller than that of 5.5 for a 10-mm-diameter pool. In other words, the strength of Marangoni convection relative to that of buoyancy convection is raised more than six times.

Figure 11 shows the flow pattern in a 4-mm pool induced by a 2-W beam of 1.5 mm diameter. Despite a number of problems associated with a small 4-mm-diameter pool, which will be described later, the flow pattern is very similar to that shown in Fig. 4 for a 10-mm pool. First, the surface flow is much faster than the return flow and there is little flow near the pool bottom. Second, the flow lines are much more closely spaced near the pool surface than in the bulk pool. Third, the centers of the cells are close to the edge of the pool surface. If flow in the 10-mm pool was not also dominated by Marangoni convection, the two flow patterns would not be very similar.

The problems encountered in the experiments with a 4-mm pool were as follows. First, the 4-mm pool was too small to measure the temperature distribution along the pool surface, vary the beam diameter over a significant range and keep the aluminum tracer particles from agglomerating. As shown in Fig. 11, the agglomerated tracer particles cause some flow lines to look more like ribbons. In fact, there would have been even more ribbons had the exposure time not been reduced from 0.625 to 0.1 s. Second, a higher magnification is required for photographing a 4-mm pool. Even with the reflex mirror in the camera already locked up, there can still be slight camera vibration to make the flow lines appear wavy in the resultant photograph, as evident in Fig. 11. Third, the radius of curvature of the pool surface was rather small in a 4-mm tube, making the pool surface highly concave, as also evident in Fig. 11.

In view of these difficulties it is almost impossible to conduct experiments with a 2-mm-diameter pool, even though the very small dynamic Bond number of 0.22 is a definite advantage. Reduced gravity, such as that provided by a drop tower or a parabolic-flight aircraft, is therefore ideal for studying Marangoni convection in a simulated weld pool. It allows the use of a pool large enough (*e.g.*, 10 mm diameter) for conducting experiments while suppressing buoyancy convection at the same time.

Conclusions

• Marangoni convection in the absence of a surface-active agent has been observed, clearly and without optical distortions, in a simulated transparent weld pool of $NaNO_3$ subjected to a defocused CO_2 laser beam.

• The Marangoni number for the simulated weld pool is close to those for welding. From the similarity law of hydrodynamics, the Marangoni convection observed in the simulated weld pool can be expected to resemble that in welding.

• Two counterrotating cells appear in the meridian plane of the pool, the maximum velocity is at the pool surface, the outward surface flow is much faster than the inward return flow, and the centers of the cells are near the pool edge. These are characteristics of Marangoni convection, and they suggest Marangoni convection dominates in the pool over gravity-induced bouyancy convection.

• Increasing the beam power and reducing the beam diameter both make Marangoni convection stronger and both move the centers of the cells closer to the pool edge, but the effect of the latter is significantly greater.

• Within the range of the experimental conditions investigated, increasing the beam power tends to reduce the depth of convection, while reducing the beam diameter tends to increase it because of the increased momentum of the returning flow.

• The use of a heater in contact with the pool surface can cause both the pool surface and the flow pattern to distort significantly.

Acknowledgments

This work was supported by NASA under Grant No. NAG8-1459.

References

1. Heiple, C. R., and Roper, J. R. 1982. Mechanism for minor element effect on GTA fusion zone geometry. *Welding Journal* 61(4): 97-s to 102-s.

2. Sahoo, P., DebRoy, T., and McNallan, M. J. 1988. Surface tension of binary metal-surface active solute systems under conditions relevant to welding metallurgy. *Metallurgical Transactions* 19B(3): 483–491.

3. Kou, S. 1987. *Welding Metallurgy*. New York, N.Y., John Wiley and Sons, pp. 91–103.

4. Kou, S. 1996. *Transport Phenomena and Materials Processing*. New York, N.Y., John Wiley and Sons, pp. 499–515, 44–48.

5. Ishizaki, K., Araki, N., and Murai, H. 1965. Penetration in arc welding and convection in molten metal. *Journal of Japan Welding Society* 34(2): 146–153 (in Japanese).

6. White, L. R., and Davis, H. T. 1967. Thermal conductivity of molten alkali nitrates. *Journal of Chemical Physics* 47(12): 5433–5439.

7. Janz, G. J. 1972. *Journal of Physical Chemistry*, Reference Data: 1(3): 583–704.

8. Preisser, F., Schwabe, D., and Scharmann, A. 1983. Steady and oscillatory thermocapillary convection in liquid columns with free cylindrical surface. *Journal of Fluid Mechanics* 126: 545–567.

9. Atomergic Chemetals Corp. 1993. Datasheet. Farmingdale, N.Y.

10. Alfa AESAR. 1999. Material safety data

sheet for $NaNO_3$. Ward Hill, Mass.
11. Schwabe, D., Scharmann, A., Preisser, F., and Oeder, R. 1978. Experiments on surface tension driven flow in floating zone melting. *Journal of Crystal Growth* 43: 305–312.
12. Rouse, H. 1978. *Elementary Mechanics of Fluids*. New York, N.Y., Dover Publications, p. 39.
13. Kou, S., and Sun, D. K. 1985. Fluid flow and weld penetration in stationary arc welds. *Metallurgical Transactions A* 16A: 203–213.
14. Lu, M., and Kou, S. 1988. Power and current distributions in gas tungsten arcs. *Welding Journal* 67(2): 29-s to 34-s.
15. Duley, W. W. 1999. *Laser Welding*. New York, N.Y., John Wiley and Sons, p. 76.
16. Mazumder, J., and Voekel, D. 1992. *Laser Advanced Materials Processing — Science and Applications*, eds. A. Matsunawa and S. Katayama. High Temperature Society of Japan. Osaka, Japan. Vol. 1, pp. 373–380.
17. Tsai, M. C., and Kou, S. 1989. Marangoni convection in weld pools with a free surface. *Internal Journal for Numerical Methods in Fluids* 9: 1503–1516.
18. Limmaneevichitr, C., and Kou, S. 1998. Flow visualization of Marangoni convection in simulated weld pool (a videotape movie), unpublished work. Madison, Wis., University of Wisconsin-Madison.
19. Kamotani, Y., Chang, A., and Ostrach, S. 1996. Effects of heating mode on steady axisymmetric thermocapillary flows in microgravity. *Journal of Heat Transfer* 118: 191–197.
20. Limmaneevichitr, C., and Kou, S. 1998. Physical simulation of thermocapillary convection in weld pools. NASA Microgravity Materials Science Conference, NASA/CP-1999-209092: 393– 398.
21. Kamotani, Y., Lee, J. H., and Ostrach, S. 1992. An experimental study of oscillatory thermocapillary convection in cylindrical containers. *Physics of Fluids* A 4: 955–961.
22. Oreper, G. M., and Szekely, J. 1984. Heat- and fluid-flow phenomena in weld pools. *Journal of Fluid Mechanics* 147: 53–79.
23. Pitscheneder, W., Ebner, R., DebRoy, T., and Mundra, K. 1996. Weld pool geometry during high power conduction mode carbon dioxide laser welding. *Trends in Welding Research*, eds. H. B. Smartt, J. A. Johnson and S. A. David. Materials Park, Ohio, ASM International.
24. Kim, W. H., Fan, H. G., and Na, S. J. 1997. Effect of various driving forces on heat and mass transfer in arc welding. *Numerical Heat Transfer, Part A* 32: 633–652.
25. Mills, K. C., Keene, B. J., Brooks, R. F., and Olusanya. 1984. Surface tension of 304 and 316 type stainless steels and their effect on weld penetration. Report of the National Physical Laboratory, Teddinton, Middlesex, U.K.
26. Limmaneevichitr, C., and Kou, S. 2000. Experiments to Simulate Effect of Marangoni Convection on Weld Pool Shape. (To be published in the *Welding Journal*.)